ELSEVIER

Journal of Nuclear Materials 313–316 (2003) 857–862

journal of nuclear materials

www.elsevier.com/locate/jnucmat

Modelling of island divertor physics and comparison to W7-AS experimental results

Y. Feng [a,*], F. Sardei [a], P. Grigull [a], K. McCormick [a], L. Giannone [a], J. Kisslinger [a], D. Reiter [b], Y. Igitkhanov [a], U. Wenzel [c]

[a] *Max-Planck-Institut für Plasmaphysik, Teilinstitut Greifswald, Wendelsteinstr. 1, 17491 Greifswald, EURATOM-Association, D-85748 Garching, Germany*

[b] *Institut für Plasmaphysik, Forschungszentrum Jülich Gmbh, EURATOM Association, Trilateral Euregio Cluster, D-52425 Jülich, Germany*

[c] *Max-Planck-Institut für Plasmaphysik, EURATOM-Association, Division Plasma Diagnostik, Mohrenstr. 41, D-10117 Berlin, Germany*

Received 27 May 2002; accepted 12 September 2002

Abstract

Extensive parameter studies have been carried out with the EMC3-EIRENE code. Major code predictions, namely the absence of high recycling prior to detachment, additional momentum losses associated with the specific island divertor geometry and the jump of the radiation at detachment transition have been verified by the W7-AS divertor experiments. Measurements and simulations are compared for high density, high power W7-AS divertor discharges and the physics related to rollover and detachment is discussed in detail. Local comparisons with the W7-AS experiment have been started with a new code version accounting for the real open-island geometry. Specifically, the observed asymmetric power unloading of the target plates at detachment transition could now be reproduced and explained. Agreement with the experiment was also found for the unexpected spatial structure of particle deposition by including classical $E \times B$ drifts into the code.

© 2003 Elsevier Science B.V. All rights reserved.

PACS: 52.65

Keywords: Edge modelling; Monte Carlo simulations; W7-AS; Island divertor; $E \times B$ drift; Stellarator

1. Introduction

A realistic prediction of the detachment physics in island divertors has become possible after implementation of the impurity transport and radiation into the EMC3-EIRENE code [1–3]. Up to now, the code has employed an island divertor model of W7-AS consisting of the true geometry of plates, baffles and walls [4] but an approximate geometry of the magnetic configuration [5]. This model configuration is very similar to the real one [4] in every respect except the weakly ergodic islands are approximated by closed ones. This approach is sufficiently realistic to describe the global plasma behaviour as long as the key geometric parameters of the island divertor, namely the connection length, the island size and the field-line pitch are correct and the magnetic structures are weakly ergodic. However, it poses a restriction for a comparison with local experimental data. This restriction has been overcome recently by implementing a new reversible field-line mapping technique in the EMC3 code, which extends the code applicability to general configurations with open islands and arbitrary ergodicity [6]. First code simulations using the real

* Corresponding author. Tel.: +49-3834 88 2000; fax: +49-3834 88 2009.

E-mail address: feng@ipp.mpg.de (Y. Feng).

0022-3115/03/$ - see front matter © 2003 Elsevier Science B.V. All rights reserved.
PII: S0022-3115(02)01463-0

configuration and addressing the physics of the particle and power depositions on the target plates are presented in this paper.

2. EMC3-EIRENE predictions

Previous EMC3-EIRENE simulations for pure hydrogen plasmas showed strong differences in transport between island divertors and standard tokamak divertors [7]. Compared to tokamaks, the downstream density n_{ed} typically exhibits a roughly linear scaling with the upstream density n_{es} indicating no high recycling and never exceeding n_{es}. The downstream temperature T_{ed} decreases with n_{es} faster than $T_{ed} \propto n_{es}^{-2/3}$ (linear regime) but slower than $T_{ed} \propto n_{es}^{-2}$ (high recycling tokamak regime). The upstream temperature T_{es} drops significantly with n_{es} even in the case of $T_{ed} \ll T_{es}$. The particle fluxes to the targets are smaller than in the two-point model even at low densities, high temperatures, indicating a significant momentum loss of the plasma ions flowing in the main channel. All these effects, which do not appear in tokamaks, are related to the prominent role of the cross-field transport arising from the combined effects of the small field-line pitch [6] ($\approx$0.001 for W7-AS compared to $\approx$0.1 for tokamaks) and the small distance of the X-point from the target plate.

After implementation of the impurity transport model into the EMC3-EIRENE code [3], a dedicated numerical transport study including intrinsic carbon impurities was carried out, aiming at the exploration of the detachment physics in the W7-AS island divertor. One basic result of these calculations was that higher upstream densities are needed to achieve detachment as compared to tokamaks, because of the additional momentum losses associated with the island divertor geometry, which have to be balanced by higher upstream pressures. Concerning the physics of detachment, major predictions of the code calculations were a jump of the radiation level and a jump of the radial position of the radiation zone at detachment transition. The first effect is due to a thermal instability associated with the two-branch characteristic of the carbon cooling rate function [6]. By increasing the impurity concentration C or the plasma density n for attached conditions, the temperature at the targets gradually drops approaching a bifurcation point where it jumps from the high temperature branch to the low temperature branch of the cooling rate function, indicating detachment transition. The second effects starts at this point and depends on the radial heat transport. As soon as the radiation capability of the impurity at the target $\mathrm{const}\sqrt{(2C\chi n^3)_{\mathrm{target}}}$ [6] exceeds the power entering the SOL, the radiation zone becomes unstable and detaches form the target. It will stop only if it finds a radial position where the local radiation capability equals the input power. No such stable position of the radiation zone has been found inside the SOL so far from both the code calculations and the bolometric measurements (see below). This process is governed essentially by the radial local power balance between cross-field transport and impurity radiation.

3. Comparison to the experiment

3.1. SOL

The first EMC3-EIRENE transport studies with self-consistent impurities covered a full upstream-density range from 1 to 6×10^{19} m^{-3}. The power entering the SOL, P_{SOL}, was gradually reduced from 1 to 0.85 MW with increasing density up to detachment to account for increasing main plasma radiation at higher densities. The transport coefficients were $D = 0.5$ m^2/s for both hydrogen and carbon, and $\chi_e = \chi_i = 3D$. A fixed total sputtering coefficient of 3% was adopted to control the impurity concentration. Fig. 1 shows a comparison of the predicted and measured [4] downstream electron density and normalised momentum loss vs. upstream density, n_{es}. The roughly linear relation between n_{ed} and n_{es} found in the code simulations throughout the density range up to rollover is verified by the experiment (Fig. 1 top) and confirms the previous predictions without impurities [7]. Density rollover is found at $n_{es} \approx 5 \times 10^{19}$ to 6×10^{19} m^{-3}, in agreement with the experiment. The additional momentum loss at low densities is also clearly verified by the experiment (Fig. 1 bottom).

A more detailed numerical study has been carried out with the input data n_{es} and P_{SOL} taken from the experiment [4] and the measured $\bar{n}_e$ as independent parameter (Fig. 2(a)). At high $\bar{n}_e$ values, P_{SOL} strongly drops due to enhanced impurity radiation in the core. The calculated n_{ed} values (Fig. 2(b)) reproduce correctly the measured upward/downward dependency on $\bar{n}_e$ including a rollover value of about 4×10^{19} m^{-3} at $\bar{n}_e \approx 2 \times 10^{20}$ to 2.5×10^{20} m^{-3}. Here the calculated core ionisation fraction, S_{core}, has a minimum, which reflects the improved neutral screening and the attached ionisation front at maximum n_{ed}. If $\bar{n}_e$ is increased further, P_{SOL} and hence the downstream temperature drop, leading to a detachment of the ionisation front, which gradually moves towards the separatrix, hereby reducing n_{ed}. At $\bar{n}_e \approx 2.8 \times 10^{20}$ m^{-3} the calculated n_{ed} drops sharply by 30% and S_{core} sharply rises from 4% to 14%, which indicates a jump of the ionisation zone to the separatrix. A jump of the radiation zone to the separatrix (not shown here) follows as soon as the radiation capability at the target exceeds the SOL input power, in agreement with the detachment physics discussed in Section 2 [6]. This

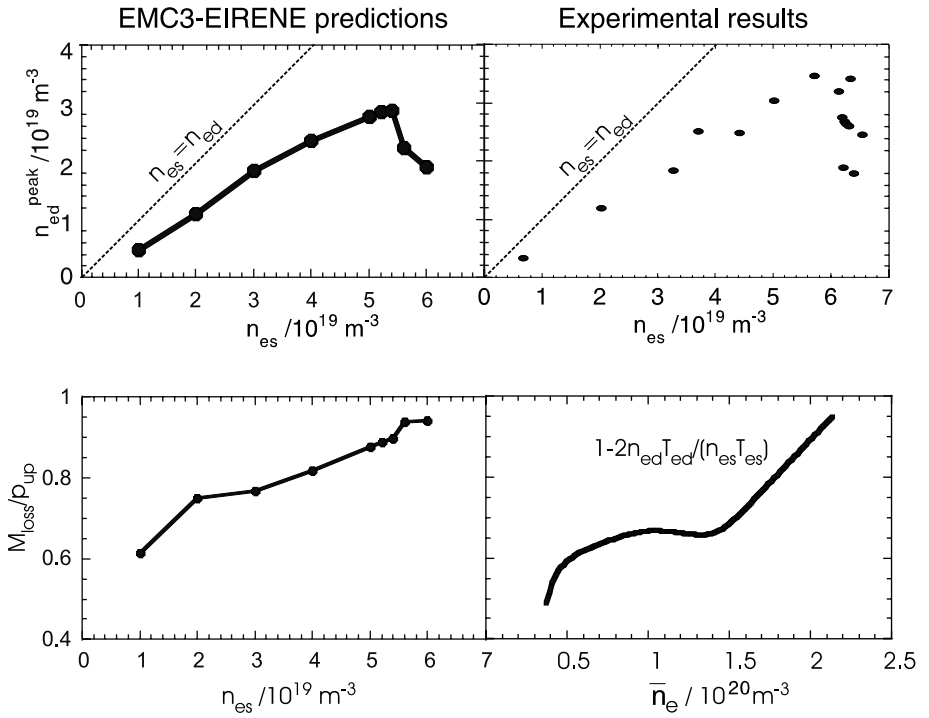

Fig. 1. Absence of high recycling and momentum loss at low densities confirmed by the experiments.

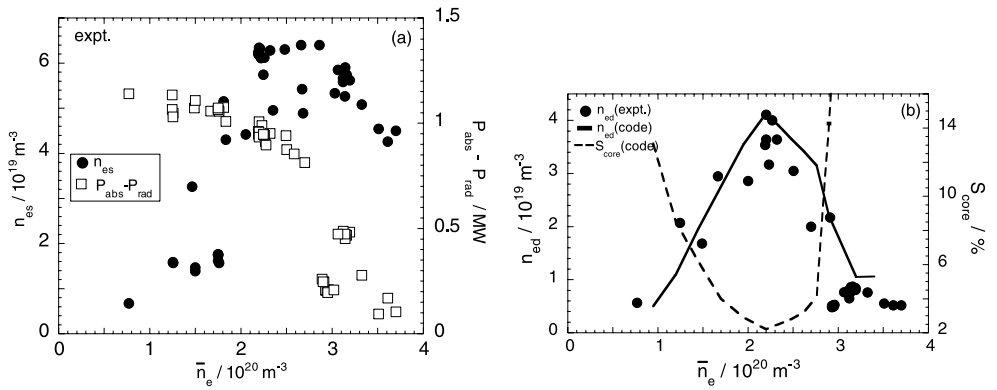

Fig. 2. Comparison of modelling and experiment for high density 2 MW NBI-heated discharges. (a) Experimental data set taken as input for EMC3-EIRENE simulations. (b) Downstream densities from experimental data and code simulations and ionisation fraction in the core from code. Drop of n_{ed} and rise of S_{core} indicate shifting of the ionisation front towards the separatrix and subsequent detachment.

jump is supported by bolometric measurements in the island divertor edge [8]. In the experiment, the n_{ed} density drop is even larger, which may be explained by a concomitant drop of the measured separatrix density, n_{es}, shown in Fig. 2(a). A sharp increase of S_{core} at detachment leads to a stronger particle outflux through the separatrix, resulting in a larger $\bar{n}_e/n_{es}$ ratio. This is a possible explanation of the measured drop of n_{es} following a gradual, feedback-controlled increase of $\bar{n}_e$.

Additionally, the EMC3-EIRENE code has predicted a jump of the carbon radiation at detachment transition (Fig. 3) [9], in agreement with bolometric measurements for a large number of quasi-stationary discharges.

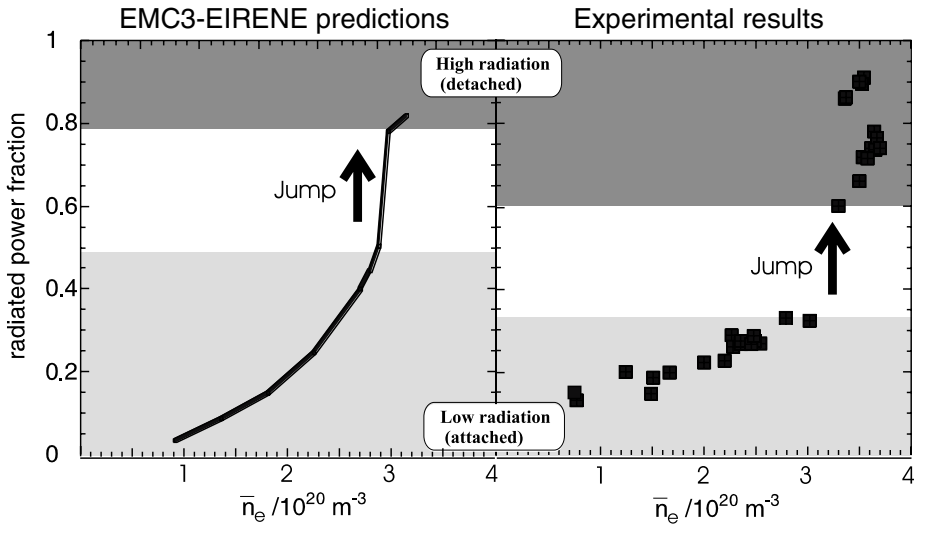

Fig. 3. Jump of carbon radiation at detachment transition.

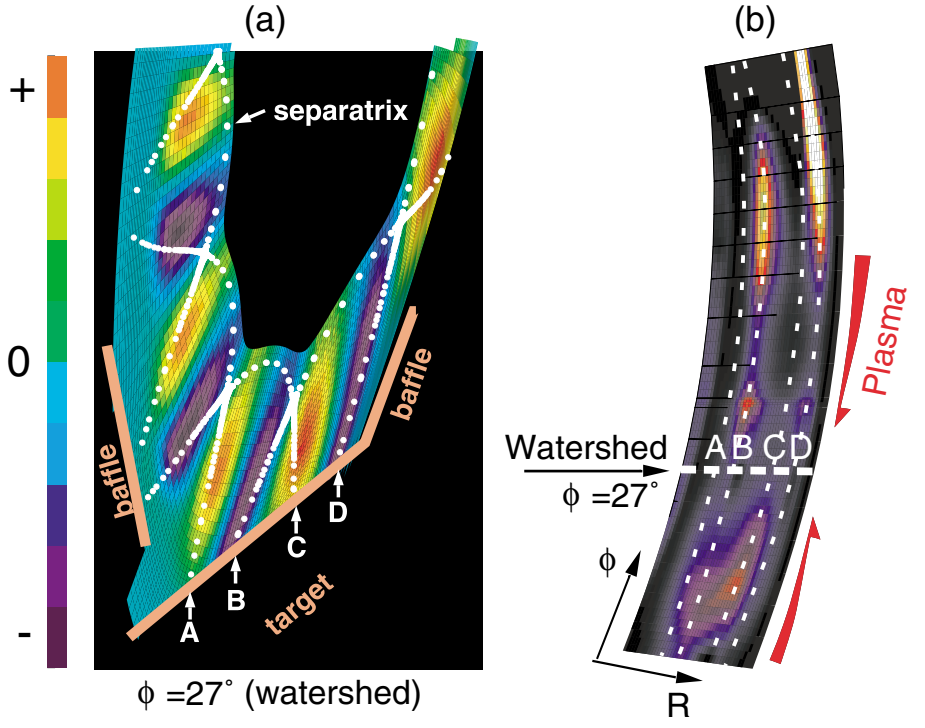

Fig. 4. Modelling of a typical attached discharge, $n_{es} = 2 \times 10^{19}$ m^{-3}, $P_{SOL} = 1$ MW. (a) Positive and negative particle flux distribution in the SOL. (b) Particle deposition on a target plate.

3.2. Target plates

After implementing the real open-island geometry of W7-AS in the EMC3 code, a realistic interpretation of local experimental data has become possible. In particular, unexpected patterns of the target particle deposition and an asymmetric power unloading of the target at detachment transition could be explained. Fig. 4(a) shows the distribution of the particle flux in the W7-AS SOL at the toroidal position of $\phi = 27°$ from code

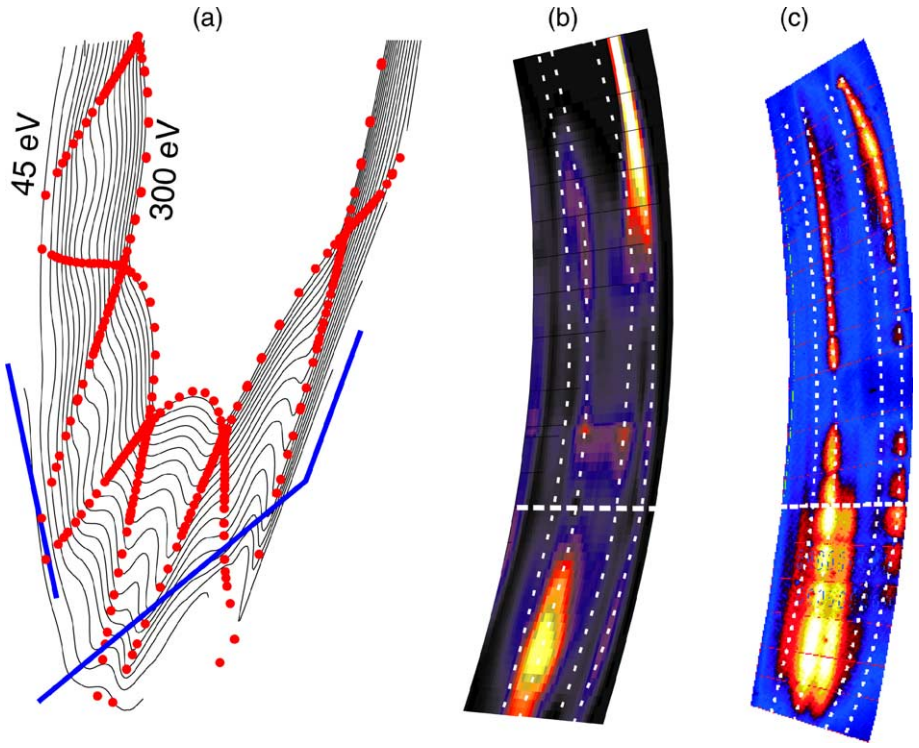

Fig. 5. Modelled particle deposition with $E \times B$ drift included and comparision to experiment. (a) Contour plot of equipotential surfaces. (b) Particle deposition from EMC3-EIRENE code with $E \times B$ drift. (c) Measured H_α distribution.

modelling for a low density, attached plasma with $n_{es} = 2 \times 10^{19}$ m^{-3} and $P_{SOL} = 1$ MW as input parameters. The poloidal sequence of positive and negative flux regions are clearly visible in the picture, their short mutual distance is one of the main reasons for the already mentioned additional losses of parallel momentum by shear viscosity. At the $\phi = 27°$ position, the target plates are bent forming a watershed which divides them in two toroidal sections. The $\phi < 27°$ and $\phi > 27°$ sections collect the plasma flows reaching the plates along the two separatrices of each island fan from the positive (strike lines through A and C) and negative (lines through B and D) toroidal directions, respectively. The expected deposition footprints along the four lines are shown in Fig. 4(b). The weak footprint along the A line reflects the relatively large distance of this plate position from the high particle flux zone (Fig. 4(a)).

In the experiment [10], however, a strong particle flow in the shadowed region (B strike line in the $\phi < 27°$ section) is typically observed (H_α distribution in Fig. 5(c)), which is evidently not consistent with the described magnetic topology. In fact, having a negative velocity, the particles from the B separatrix (Fig. 4(a)) should strike the plates on the $\phi > 27°$ section. Particles with positive velocity from the neighbouring island fans A and C can enter this shadowed region by diffusion, which, however, cannot lead to a shift of the maximum flux location. Such a shift can only originate from a cross-field convective flow.

$E \times B$ drift effects in a W7-AS island divertor configuration for low density discharges have already been modelled with the EMC3-EIRENE code during predivertor investigations with inboard target plates [11]. In that study, measured poloidal density asymmetries could be reproduced qualitatively by a very simple model neglecting potential variations on island surfaces. The model used in the present study goes a step further by integrating the parallel momentum equation for electrons

$$j_\parallel = \sigma_\parallel \left[\frac{1}{en} (b \cdot \nabla n T_e + n C_e b \cdot \nabla T_e) - b \cdot \nabla \Phi \right]$$

to determine the 3D potential distribution. Cross-field electric currents are still neglected, which implies constant parallel currents along the field lines. $\sigma_\parallel$ is the Spitzer conductivity. Two boundary conditions at the grounded target plates linked to the plasma by the standard sheath potential are used to determine $j_\parallel$ and the integration constant for Φ. This model takes fully into account the strong link of the potential to the parallel temperature gradient, which is a quite robust parameter for island divertor configurations. A more

sophisticated model has been used in [12], however only on a strongly simplified 2D model island divertor geometry. In the present model, the $E = -\nabla\Phi$ field is determined from equipotential surfaces (Fig. 5(a)) and the corresponding $E \times B$ drift terms are included in the continuity and momentum equations. These drifts destroy the stellarator symmetry, wherefore the toroidal computational domain had to be extended from one half to one full period. Furthermore, Φ is averaged along field lines over one field period in order to improve the Monte Carlo statistics. The calculations show that the $E \times B$ drift causes a poloidal phase shift of the parallel particle flow from the C to the B strike line (Fig. 4(b)) in agreement with the observed patterns in Fig. 5(c).

Impurity radiation removes the power load to the targets. However, the unloading of the plates is not homogeneous, especially at detachment transition [10]. Typically the plasma does not detach at the D strike zone (Fig. 4(b)) in the $\phi > 27°$ section of the plates. This behaviour is reproduced by the simulations [13] and can be explained as follows. The $\phi > 27°$ strike zones are magnetically connected to the outboard side of the torus, wheras the strike zones for $\phi < 27°$ are magnetically connected to the inboard side. In particular, the D strike zone has the shortest connection length to the outboard side. Here the parallel power flux to the targets is higher than at the inboard side for two reasons. First the temperature level is higher due to the radial field line compression which favours the radial heat transport. Secondly, at detachment transition the carbon impurity radiation is localised in the poloidal zone with lowest temperatures, i.e. at the inboard side. This is confirmed by code calculations and supported by bolometric measurements [8]. The reduced drop of the parallel power flux to the D strike zone of the plates is evidently not sufficient to achieve detachment there.

References

[1] Y. Feng, F. Sardei, J. Kisslinger, J. Nucl. Mater. 266–269 (1999) 812.
[2] D. Reiter, Technical Report Jül-1947, KFA Jülich, Germany, 1984.
[3] Y. Feng, F. Sardei, J. Kisslinger, D. Reiter, Y. Igitkhanov, in: 28th EPS Conference, Madeira, 2001.
[4] P. Grigull et al., Plasma Phys. Control. Fusion 43 (2001) A175.
[5] Y. Feng, F. Sardei, J. Kisslinger, D. Reiter, Y. Igitkhanov, Contrib. Plasma Phys. 42 (2–4) (2002) 187.
[6] Y. Feng, F. Sardei, P. Grigull, K. McCormick, J. Kisslinger, D. Reiter, et al., Plasma Phys. Control. Fusion 44 (2002) 611.
[7] Y. Feng, J. Kisslinger, F. Sardei, in: 26th EPS Conference, Maastricht, 1999.
[8] L. Giannone et al., Plasma Phys. Control. Fusion 44 (2002) 2149.
[9] K. McCormick et al., Phys. Rev. Lett. 89 (2002) 015001.
[10] K. McCormick et al., in: 13th International Stellarator Workshop, Canberra, 2002.
[11] Y. Feng, F. Sardei, P. Grigull, G. Herre, W7-AS Team, J. Nucl. Mater. 266–269 (1999) 928.
[12] X. Bonnin, R. Schneider, D. Coster, V. Rozhansky, S. Voskoboynikov, J. Nucl. Mater 290–293 (2001) 829.
[13] P. Grigull et al., these Proceedings.